Investigating of Flow Field and Power Performance on a Straight-blade Vertical Axis Wind Turbine with CFD Simulation

Yanfeng Zhang[1], Zhiping Guo[2], Xiaowen Song[2], Xinyu Zhu[2], Chang Cai[3] and Qing'an Li[3*]

[1]*College of Science, Inner Mongolia University of Technology, Hohhot 010051, China.*
[2]*College of Mechanical Engineering, Inner Mongolia University of Technology, Hohhot 010051, China.*
[3]*Institute of Engineering Thermophysics, Chinese Academy of Sciences, Beijing 100190, China.*

Authors' contributions

This work was carried out in collaboration among all authors. All authors read and approved the final manuscript.

Original Research Article

ABSTRACT

Forecasting the power performance and flow field of straight-blade vertical axis wind turbine (VAWT) and paying attention to the dynamic stall can enhance more adaptability to high turbulence and complicated wind conditions in cities environment. According to the blade element-momentum theory, the force of blade is analyzed in one period of revolution based on the structural characteristics of straight blade airfoil. The power performance of VAWT obtained by computational fluid dynamics (CFD) simulation is compared with experiment to estimate the accuracy about the numerical simulation results. As a result, the trend of average value of simulation C_{power} is entirely consistent with the value of experiment data, and the extreme value of average C_{power} of VAWT is 0.225 for tip speed ration (TSR) λ=2.19 when the freestream velocity is 8 m/s. The flow separation around the blade surface also gradually changes with the azimuth angle increasing, and the maximum pressure difference on the blade surface appears in the upstream. In the case of high leaf tip velocity, the synthetic velocity is much larger than the incoming wind velocity, and the angle

_____

Corresponding author: E-mail: liqingan@iet.com;

of synthetic velocity increases slightly with the increase of blade tangential velocity. Thus, the angles of attack are very close in two TSRs λ=2.19 and 2.58. The research provides a computational model and theoretical basis for predicting wind turbine flow field to improve wind turbine power performance.

Keywords: VAWT; CFD simulation; TSR; flow field; power performance.

1. INTRODUCTION

Fossil energy is gradually decreasing with the rapid growth of energy consumption and economic growth. It has forced governments to develop clean energy [1]. Wind energy, clean and abundant renewable energy, has been focused by governments all over the world [2]. Therefore, as the main wind energy conversion equipment, wind turbine has become a hot research field to improve the overall performance [3]. In comparison of the horizontal axis wind turbine (HAWT), the vertical axis wind turbine (VAWT) is more suitable for application in same remote mountain areas and cities environment, which had attracted more and more attentions to research on aerodynamic characteristics of VAWT [4].

The main methods for researching the flow field and power performance of VAWTs are numerical simulation and wind tunnel experiment [5]. Li Q et al. predicted aerodynamic performance of a straight-blade VAWT by using wind tunnel and CFD simulation [6]. The dynamic stall phenomenon cannot be ignored in the design and control of a VAWT, as which impact aerodynamic load, operational process and wake dynamics [7-8]. This same conclusion is obtained in reference [9]. Li Q et al. measured the wind speed around the straight-blade VAWT by laser doppler velocimetry (LDV) in the wind tunnel. The results show that the turbulence intensity decreased with the increase of the TSRs in the flow field [10]. The LES approach in CFD was used to test the performance of Smagorinsky, dynamic k-equation, and dynamic Lagrangian turbulence models. In addition, the near-wake generated for the VAWT was simulated using the actuator line model (ALM) to study the overall wake situation [11]. The blades tip vortex characteristics were investigated in the velocity fields at different TSRs by the Q-criterion iso-surface and shear-stress transport (SST) k-ω turbulence model [12]. The same issues are approached in reference [13]. Meanwhile, the influence of pitch Angle and Angle of attack on dynamic performance and aerodynamic characteristics of VAWT can also be obtained

through CFD analysis under different TSR [14]. This same conclusion is approached in reference [15]. Hara Y et al. studied the influence of arms of different sections on the VAWT and found that the drag torque of the rotor of the airfoil arm added to the blade became larger than that of other arms [16].

At present, some wind turbine structure optimization measures, such as airfoil profile modification, tubercle leading edge (TLE), and upstream deflector, were implemented to improve efficiency of VAWTs [17-18]. This same conclusion is approached in reference [19]. Kirke et al. [20] found that high solidity can cause the self-starting performance of VAWT to increase under low TSR [21]. These measures are based on the output power of the VAWT and do not consider the correlation between the variation of aerodynamic load on the blade surface and the blade output performance.

In short, the researchers have made significant achievements on the power performance of the straight-blade VAWT. However, less research has been done on the effects of the rotate velocity under different TSRs on the power performance of VAWT. Therefore, in this paper, the flow field distribution and aerodynamic performance around the wind turbine blade are studied through CFD numerical simulation and wind tunnel test, and to reveal the relevant characteristics of the aerodynamic characteristics of the straight-blade VAWT under different TSRs, in order to optimize the blade airfoil parameters and improve the power performance of VAWT to provide theoretical support.

2. STRAIGHT-BLADE VAWT STRUCTURE

The wind wheel includes blades, blade brackets and a rotary shaft. When the incoming wind velocity blows through the wind wheel, in Fig. 1, the blades rotate around the rotor shaft under the action of the wind energy, and drive the generator to output electricity [5]. As the main part of VAWT for converting wind energy into mechanical energy, the blade with good flow field and aerodynamic performance is the key factor

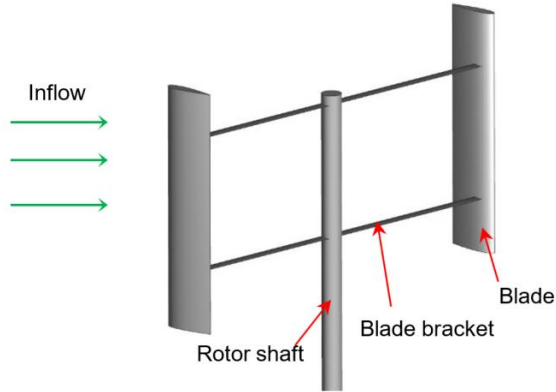to ensure the output performance of wind turbine [9].

Fig. 1. The straight-blade VAWT structure

Due to the blade of straight-blade VAWT is designed with constant cross-section design. According to the blade element theory, the wind turbine blade is divided into many equivalent micro segments along the spanwise direction. The main wind velocity U_0 is incoming from left to right, and the tangential velocity of blade V is the wind turbine rotational velocity. The synthetic flow velocity W is
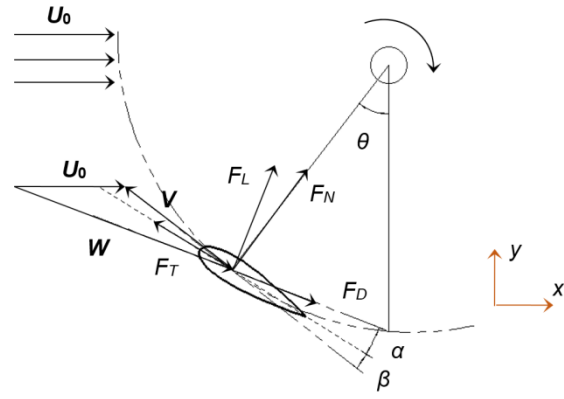
$$W = U_0 + V \qquad (2.1)$$

Fig. 2. Blade force analysis

The component F_x of the aerodynamic force in the x direction is the thrust force, and the component F_y in the y direction is the lateral force. F_x and F_y are decomposed into the tangential force (F_T) along the chord direction and the normal force (F_N) perpendicular to the chord direction. Then

$$F_T = F_y \cdot \sin\theta - F_x \cdot \cos\theta , \ F_N = -F_y \cdot \cos\theta - F_x \cdot \sin\theta \qquad (2.2)$$

In Table 1, the following parameters are dimensioned to obtain the coefficients to better express the aerodynamic characteristics of VAWT blades.

Table 1. Dimension load factor

Load type	Formula	Load type	Formula
Pressure coefficient	$C_P = P/(0.5\rho W^2)$	TSR	$\lambda = \omega R/U_0$
Torque coefficient	$C_Q = Q/(0.5\rho DHU_0^2 R)$	Power coefficient	$C_{power} = Q\omega/(0.5\rho DHU_0^3)$

where, ρ is the air density (kg/m^3), and R is the radius of gyration ($R=D/2$), ω is the angular velocity of VAWT rotor shaft (rad/s), H is the span length of wind turbine blade (m).

3. NUMERICAL MODEL

3.1 Physical Model of VAWT

A straight-blade VAWT is employed to research the aerodynamic characteristics in this paper, which is reference [14]. The VAWT parameters are shown in Table 2.

Table 2. Parameters of straight-blade VAWT

Parameter	Value	Parameter	Value
Blade airfoil	NACA0021	Pitching angle (β)	6°
Blade number (N)	2	Rotor diameter (D)	2.00 m
Span length (H)	1.20 m	Shaft diameter (d)	0.15 m
Chord length (c)	0.265 m	Shaft length (h)	1.2 m

3.2 Computational Domain & Mesh Setup

The flow field and aerodynamic characteristics of wind turbine are numerically simulated by using structural grid method. As shown in Fig. 3(a), the calculation domain of VAWT model is divided into outer and inner zones with diameter of $2D$ and height of $1H$. Dimensions of outer zone are $20D$ in length, width and height of x-axis, $10D$ in y-axis and $2H$ in z-axis. It is a prismatic boundary layer on the blade surface. Because of the large wind speed gradient and pressure difference near the blade, the grid on the blade surface has been intensively processed to improve the calculation accuracy [21]. The maximum y^+ value on the blade surface is less than 1, which is considered to be the refinement of the boundary layer cells [22]. The first boundary layer thickness is 0.02mm with a growth ratio of 1.25.

The inlet is set as the wind speed inlet (U_0=8m/s) and the outlet is set as the pressure outlet with zero relative pressure. The turbulent intensity of the incoming wind velocity is 1% and the turbulent length scale is 0.014mm. The sliding wall condition is used to the remaining four boundaries of the outer zone, while the non-sliding wall condition is assigned to the blade and the shaft surface [23]. The interface condition is applied to the contact surfaces between inner and outer zone.

3.3 Solver Setting

When the wind turbine is rotating steadily, the airflow is separated on the blade surface, and the airflow velocity is lower than 0.3 Mach, which means airflow can be considered as an incompressible gaseous fluid in the computational domain [24]. The Shear Stress Transport (SST) k-ω turbulence model, which deals with flexible wall boundaries and effectively stabilizes the results, is used to deal with boundary layer flows and modify the turbulence formula [9]. Considering the unsteady implicit isolated flow model and the discrete differential equation, the semi-implicit method (SIMPLE) of pressure correlation equation is used to solve the pressure-velocity coupling problem. When the residual is equal to or less than 10^{-3}, the simulation results are convergent.
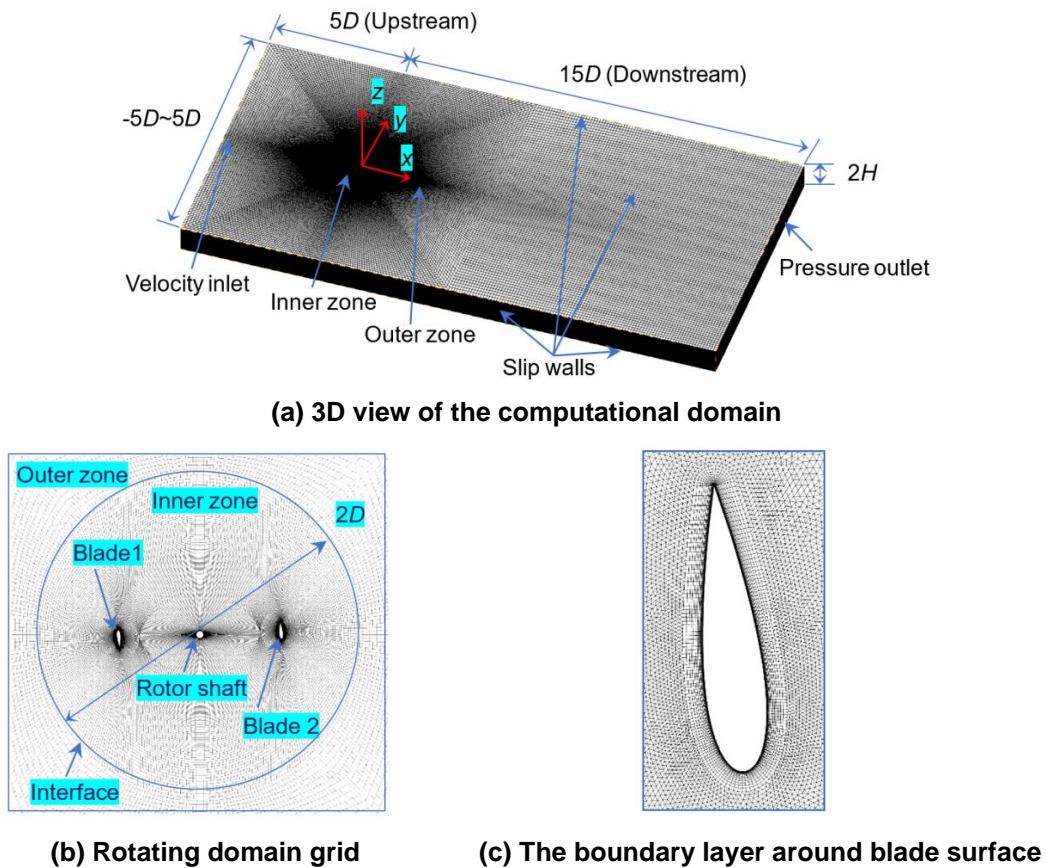

(a) 3D view of the computational domain

(b) Rotating domain grid   **(c) The boundary layer around blade surface**

Fig. 3. The computational domain with sizes of VAWT model

4. VERIFICATION OF CFD MODEL

4.1 Sensitivity Test of Grid Size

The grid sensitivity test of grid quality and quantity have an important influence on the reliability and validity of computational results. The grid sizes in the blade surface determines the surface pressure distribution and the flow field around the blade. Here three maximum grid sizes in the blade surface are set: 4mm (Intensive), 8mm (Medium) and 12mm (Coarse). The power coefficient (C_{power}) at the $λ$=2.19 is selected as the evaluation criterion. The power coefficient C_{power} of experiment values from a published paper [14].

The grid sizes, grid numbers and the value of C_{power} in three cases are shown in Table 3. As can be seen, the relative error in medium case is only 6.16%, which presents the value of C_{power} most close to the experimental data. The relative error from the intensive case to the medium case is only 1.9%, but the gird numbers is increased about 2 million, which indicates that further refinement of mesh will increase more calculations, and only play a smaller role in the calculation. Hence, the medium case is chosen as the final simulation grid by considering the efficiency and accuracy of the simulation in the present study.

4.2 Comparison with Experimental Result

In this part, the calculation results of this CFD model will be verified by using experimental data of VAWT from a published paper [14]. The main of wind tunnel test equipment is listed in Fig. 4, and the use method of equipment is given in references [5] and [6]. More detailed parameters of experimental equipment can be found in the reference [10].

According to the experiments, the simulations are designed at different TSRs and a rated wind speed of 8 m/s. The power coefficient (C_{power}) is chosen a significant parameter to reflect distinctly the utilization ratio of wind energy of VAWTs, which is used to test the CFD model. Fig. 4 shows the comparison of simulated and experimental data in different TSRs. In the Fig. 5, the trend of average value of simulation C_{power} is entirely consistent with the value of experiment data. The influence of wind turbine support structure is ignored in the CFD model, resulting in the simulated C_{power} slightly larger than the experimental value. At the same time, it is found

that the minimum difference of the two data is 0.013 at $λ$=2.19, and the maximum difference is 0.037 at $λ$=2.58. The maximum of the simulation and experiment is at $λ$=2.19, which means when the freestream velocity is 8 m/s, the angular velocity that generates the maximum power output is the rated speed of the wind turbine with this type of parameter.
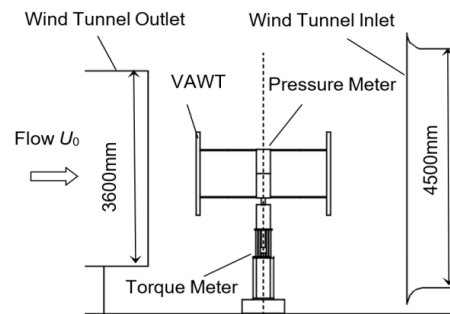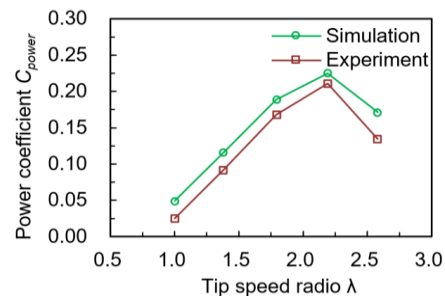

Fig. 4. Wind tunnel experiment

Fig. 5. The average power coefficient of VAWT with two blades

Fig. 6 compares the instantaneous power coefficient for single blade between two results data at $λ$=2.19. The simulated C_{power} overall trend is acceptable relative to the experiment. In the region 0°<$θ$<44° and 310°<$θ$<360°, the experimental results are larger than the simulation results, and the maximum relative error is 0.15 at $θ$=355°. The trend of C_{power} for simulation is almost coincided with the experimental data in the region 40°<θ<240°, and the both maximum value of two results appear in the same azimuth angle $θ$=105°. As shown in the Fig. 5 and Fig. 6, there are some differences between simulation and experiment, which are caused by many factors, such as physical model simplification, CFD model selection, mesh quality, energy loss, etc. [11,14]. While there are differences, those differences are acceptable. Therefore, the CFD model has certain accuracy and reliability, which can be applied to the subsequent simulation in this paper.

Table 3. Calculation parameters

Grid sizes	Grid density	Grid numbers	Simulation C_{power}	Experiment C_{power}	Relative error
4 mm	Intensive	5944720	0.228	0.211	8.06%
8 mm	Medium	3928734	0.224	0.211	6.16%
12 mm	Coarse	2251334	0.195	0.211	-7.58%

5. RESULTS AND DISCUSSION

5.1 Comparison of Power Coefficient

The instantaneous single blade power coefficient (C_{power}) is discussed at different λ in this section. In Fig. 7, the change trend of the C_{power} curves of single blade for straight-blade VAWT are basically coincident. The maximum value of power coefficient is 0.51, 0.75 and 0.70, for λ=1.38, 2.19 and 2.58, respectively, which occurs respectively at θ=105°, 110° and 115°. Moreover, the peak power coefficient are 0.13, 0.245, 0.20 in downstream domain at λ=2.58 for λ=1.38, 2.19 and 2.58, and the corresponding azimuth angle is 285°, 270°and 265°, respectively. The maximum value occurs later during one rotational period at high TSR. The Fig. 6 can also explain why the average power coefficient at λ=2.19 is largest relative to other TSRs.
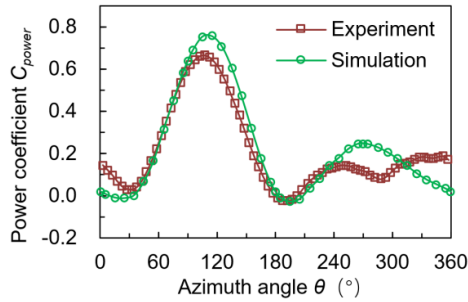

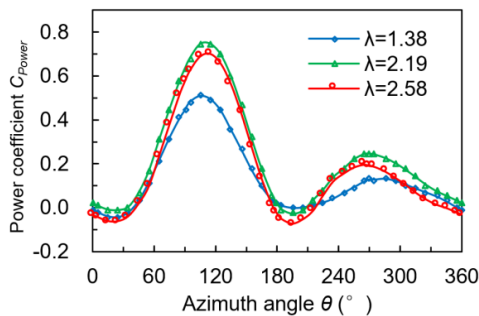**Fig. 6. The instantaneous power coefficient of single blade (λ=2.19)**

Fig. 7. The power coefficient for single blade

5.2 Comparison of Pressure Distribution

In Fig. 8 (a), at θ=0° in all three cases, the pressure coefficient is positive in the region [0, 0.15c] on the pressure side (inner side) and the negative pressure occurs in other regions of three TSRs. There is no obvious change in pressure difference in the section [0.15c, 1.0c] between the pressure side and suction side at λ=1.38. The differential pressure coefficient between the inner side and outer side in the region [0, 0.3c] is bigger than that in other parts at λ=2.19 and 2.58. In Fig. 8 (b) (θ=60°), the maximum positive value of pressure coefficient is 5.87 at λ=1.38 or 14.8 in both the two case (λ=2.19 and 2.58) on the inner side near the leading edge. The maximum negative value of pressure coefficient is -20.1 at the position of 0.1c of λ=2.19 and 2.58. In Fig. 8 (c) (θ=120°), the pressure difference between the inside and outside is gradually reduced in three cases. The pressure coefficient on the inner side has no obvious change in the region [0.3c, 0.9c] at λ=1.38.

At θ=180° (Fig. 8 (d)), the positive pressure coefficient only exists at the leading edge in the section [0, 0.04c] in the three cases, and the value of pressure coefficient on the both inner and outer side are very closely related in the section [0.1c, 1.0c]. In Fig. 8 (e), the extremums of negative pressure coefficient on the outer side (λ=1.38) occur at the position of 0.0c with a value of -12.4 and at the position of 0.09c with a value of -8.4. This can be shown in Fig. 8 (f) (λ=1.38, θ=240°), where a detached vortex near the position of 0.09c can be found at the leading edge. When it comes to θ=300° from θ=240° (Fig. 8 (f)), the pressure distributions on both sides are similar to those two degrees. The maximum differential pressure coefficient occurs at the leading edge at λ=2.58 with a value of 58.2, at λ=2.19 with a value of 48.6, and at λ=1.38 with a value of 13.2. Besides, pressure coefficient does not change significantly in the section [0.4c, 1.0c] for these two azimuths in the three cases.

In upstream domain (Fig. 8 (a-c)), a large differential pressure range appears in the section

[0, 0.5c] in the azimuth section [60°, 120°]. In downstream domain (Fig. 8 (d-f)), a large differential pressure range appears in the section [0, 0.3c] in the azimuth section [240°, 300°].

5.3 Comparison of Vorticity Field

As described above, when determining the blade profile, the change of azimuth leads to the change of power coefficient and affects the vorticity field on the blade. This change is not obvious, and small-scale vortices can't be accurately captured. The Fig. 9 shows the vorticity field at a specific azimuth interval (60°) in three cases, illustrating the development trend of vorticity around a blade. Therefore, the change of vorticity is unspecific, and the scale of some vortices is too small to be accurately displayed.

When λ=1.38, the separation vortex can be found on the outside of the blade, and starts to fall off slowly at θ=0°. In the azimuth profile [0°,

180°], the position of the inner separation flow moves from the trialing edge to the leading edge, and the moving direction of the inner space separation position is just the opposite. At θ=180 °, a large-scale bound vortex appears at the chord position 0.3c at the inside side of the blade and falls off the blade surface at θ=240 °. A large-scale vortex is observed at the chord position 0.4c at the outside the blade surface at θ=240°, and completely sheds from the blade surface at θ=300°. For λ=2.19 and λ=2.58, the flow development trend is highly consistent under the same azimuth. At θ=0°, the growth vortex occurs on the outside of the blade surface towards the trailing edge, and becomes extremely elongated around θ=60°. The slender vortex starts to convert to the inside of blade at θ=90°, and becomes shorter around θ=180°. In the azimuthal angle profile [180°, 300°], the trailing edge of the blade is always attached with growing slender vortices. Under the same azimuthal angle, the extension length of vortex at λ=2.58, is slightly greater than at λ=2.19.
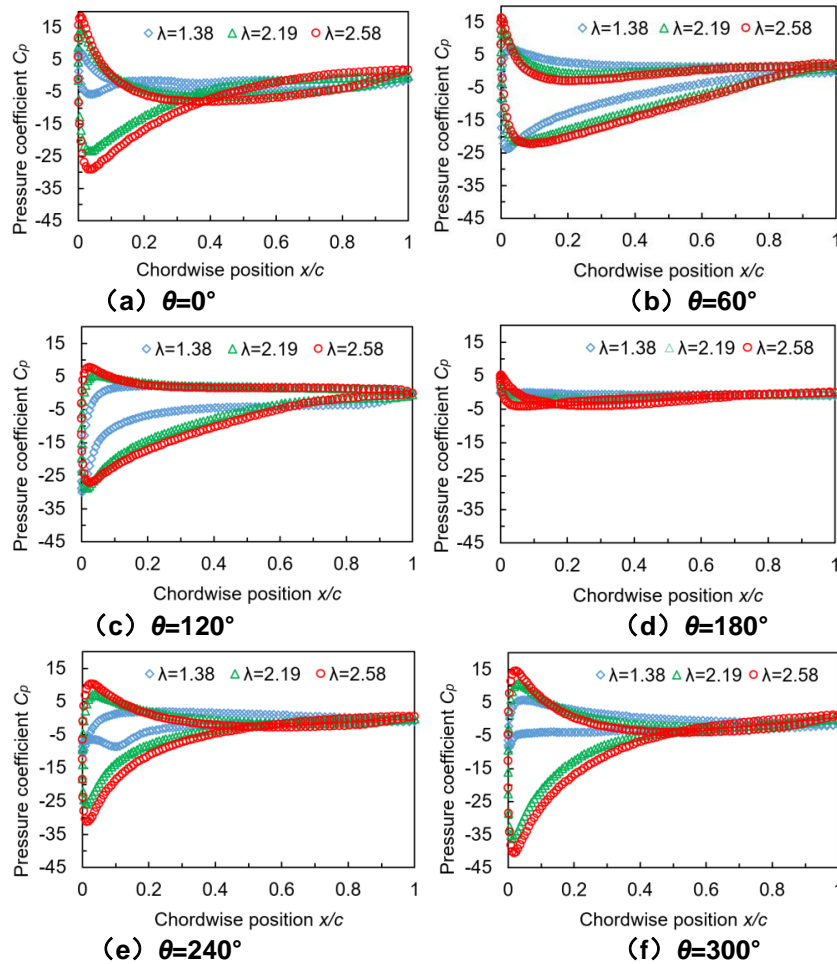
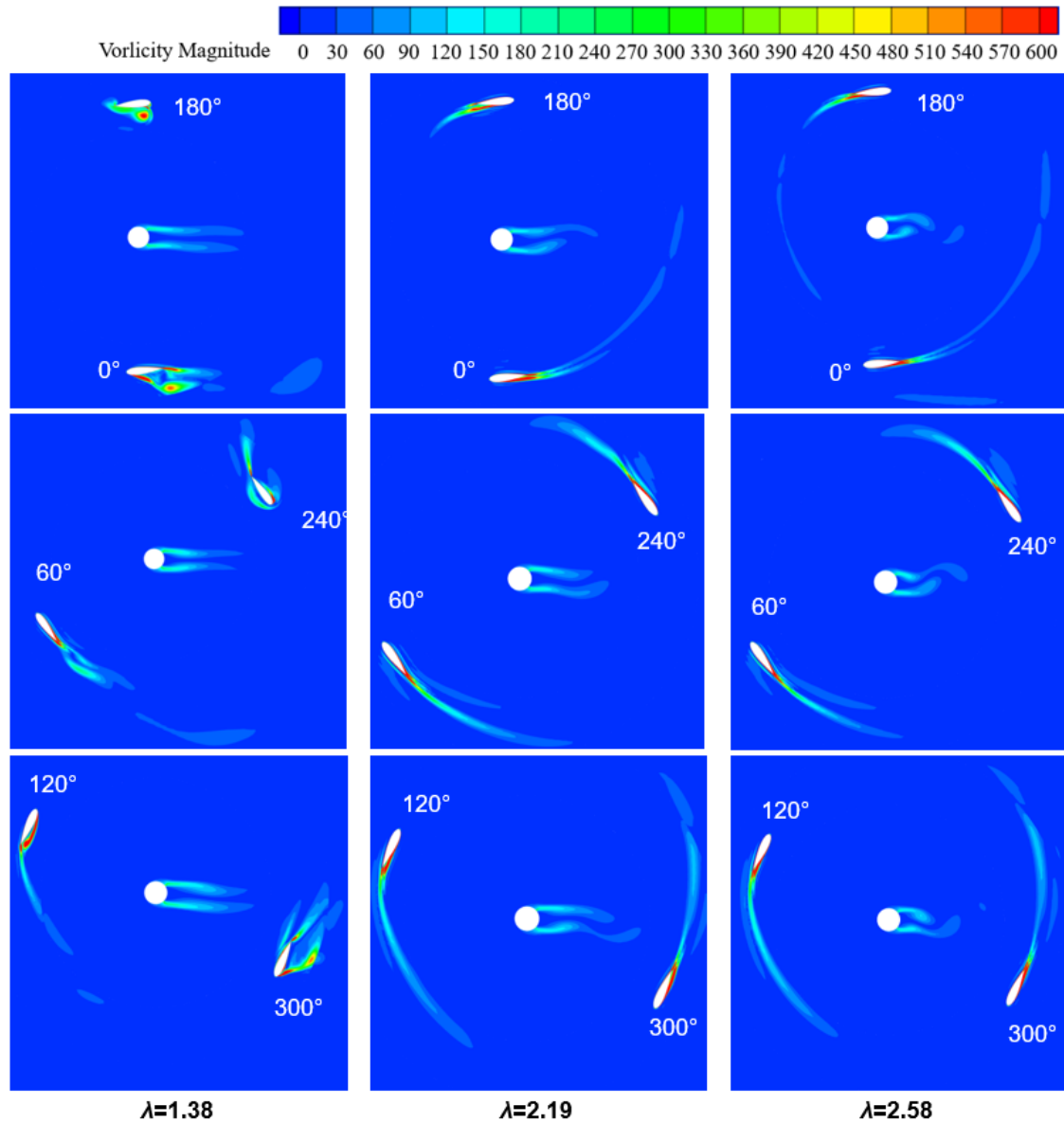**Fig. 8. Pressure coefficient distribution on the mid-span section of one blade**

Fig. 9. Instantaneous contours of vorticity magnitude on the mid-span section of the VAWT blade

In contrast with the different TSRs, the flow field distribution is distinctly distinguished by the relative motion between the airflow and blades, and the rotor of a VAWT may be subjected to more types of vane vortex interactions. The iso-surface contours of the Q-criterion colorized by the norm of the synthetic velocity (*U*) for *Q*=100 in three case (*λ*=1.38, 2.19 and 2.58) are shown in Fig. 10 for per 60° azimuth.

At the low TSR (*λ*=1.38) (Fig. 10 (a)), it is obvious that the dynamic stall occurs on the

outer sides of two blades. A large number of large vortices fall off from the blade trailing edge to the wake, which is very important in transporting the momentum and transferring energy of the turbulence, and also influence the pressure distribution and the aerodynamic forces. Meanwhile, the blade is in dynamic full stall state at *θ*=180°. Under the action of the incoming wind speed, the blade wake begins to affect the flow field outside of blade from *θ*=180° to *θ*=240°.
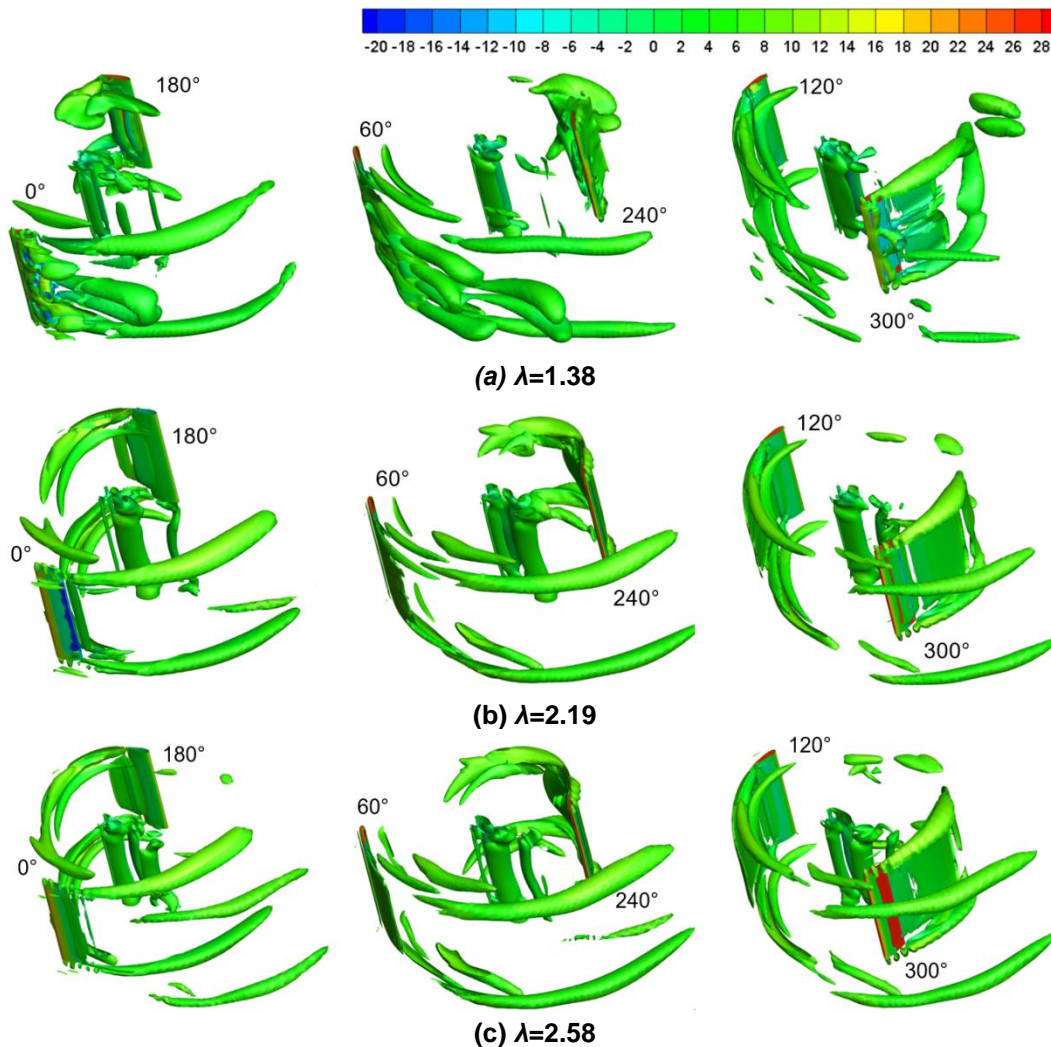
Fig. 10. The iso-surface contours of Q-criterion colorized by norm of synthetic velocity (U) for Q=100

In Fig. 10 (b-c), many vortices around and away from the blades are similar in both cases (λ=2.19 and 2.58), and are shedding from the blade trailing edge. The range of azimuth, at which the blade experiences the dynamic stall in two cases, is less than that in case of λ=1.38. In addition, the wakes of tip vortex in two cases are longer than that in case of λ=1.38 at same azimuth. On the one hand, the synthetic flow velocity (W) is much greater than the incoming wind speed (U) in the case of high TSR, and the angle of synthetic flow velocity (φ) is slightly increasing with the blade tangential velocity growing, thus the angles of attack are very close in two case λ=2.19 and 2.58. On the other hand, a lot of small-scale vortices separation occurs near the trailing edge, resulting the flow field on the outside of blade locally stall. Therefore, the

instantaneous pressure distribution on the blade surface is very similar to the aerodynamic distribution trend of the rotor for high TSRs.

6. CONCLUSION

Based on wind tunnel experiment and CFD simulation technology, this paper studies the aerodynamic performance characteristics of VAWTs under different TSRs. The results are as follows.

(1) The trend of average value of simulation C_{power} is entirely consistent with the value of experiment data. The maximum average C_{power} of VAWT is at λ=2.19, which means TSR is λ=2.19 at 8 m/s wind speed as the corresponding rotation rate is rated rotation

rate. The curve of simulation C_{power} of single blade is almost coincided with the experimental data in the region $40°<θ<240°$, and the both maximum value of two results appear in the same azimuth angle $θ=105°$.

(2) The flow separation changes gradually on blade surface with the increase of azimuth Angle. The maximum pressure difference on blade surface appears upstream. Therefore, the C_{power} of the straight-blade VAWT is mainly contributed by the wind energy in upstream.

(3) In the case of high TSR, the synthetic flow velocity (W) is much larger than the incoming wind velocity (U), and the synthetic flow angle (φ) increases slightly with the increase of the blade tangential velocity. Thus, the angles of attack are very close in two case $λ=2.19$ and 2.58. A large number of small-scale vortexes were separated near the trailing edge of the blade, and the flow field outside the blade was partially stalled.

ACKNOWLEDGEMENTS

COMPETING INTERESTS

Authors have declared that no competing interests exist.

REFERENCES

1. Chehouri A, Younes R, Ilinca A, Perron J. Review of performance optimization techniques applied to wind turbines. Applied Energy. 2015;142:361-388.

2. Georgilakis PS. Technical challenges associated with the integration of wind power into power systems. Renewable and Sustainable Energy Reviews. 2008;12: 852-863.

3. Dessoky A, Lutz T, Bangga G and Krämer E. Computational studies on Darrieus VAWT noise mechanisms employing a high order DDES model. Renewable Energy. 2019;143:404-425.

4. Wu G, Zhang L and Yang K. Development and validation of aerodynamic measurement on a horizontal axis wind turbine in the field. Applied Sciences. 2019;9:1-21.

5. Li Q, Maeda T, Kamada Y, Shimizu K, Ogasawara T, Nakai A, Kasuya T. Effect of rotor aspect ratio and solidity on a straight-bladed vertical axis wind turbine in three-dimensional analysis by the panel method. Energy. 2017;121:1-9.

6. Li Q, Maeda T, Kamada Y, Murata J, Furukawa K and Yamamoto M. The influence of flow field and aerodynamic forces on a straight-bladed vertical axis wind turbine. Energy. 2016;111:260-271.

7. Zanon A, Giannattasio P and Simão Ferreira CJ. Wake modelling of a VAWT in dynamic stall: impact on the prediction of flow and induction fields. Wind Energy. 2015;18:1855-1874.

8. Guo Y, Liu L-q, Li Y, Xiao C-s and Tang Y-g. The surge-heave-pitch coupling motions of the Φ-type vertical axis wind turbine supported by the truss Spar floating foundation. Journal of Hydrodynamics. 2018;31:669-681.

9. Lei H, Zhou D, Bao Y, Chen C, Ma N and Han Z. Numerical simulations of the unsteady aerodynamics of a floating vertical axis wind turbine in surge motion. Energy. 2017;127:1-17.

10. Li Q, Maeda T, Kamada Y, Murata J, Furukawa K and Yamamoto M. Measurement of the flow field around straight-bladed vertical axis wind turbine. Journal of Wind Engineering and Industrial Aerodynamics. 2016;151:70-78.

11. Mendoza V, Bachant P, Ferreira C and Goude A. Near-wake flow simulation of a vertical axis turbine using an actuator line model. Wind Energy. 2019;22:171-188.

12. Yang Y, Guo Z, Zhang Y, Jinyama H and Li Q. Numerical investigation of the tip vortex of a Straight-bladed Vertical Axis Wind Turbine with double-blades. Energies. 2017;10:1-18.

13. Ma N, Lei H, Han Z, Zhou D, Bao Y, Zhang K, Zhou L and Chen C. Airfoil optimization to improve power performance of a high-solidity vertical axis wind turbine at a moderate tip speed ratio. Energy. 2018; 150:236-252.

14. Yang Y, Guo Z, Song Q, Zhang Y and Li Q. Effect of blade pitch angle on the

aerodynamic characteristics of a straight-bladed vertical axis wind turbine based on experiments and simulations. Energies. 2018;11:1-15.

15. Elsakka MM, Ingham DB, Ma L and Pourkashanian M. CFD analysis of the angle of attack for a vertical axis wind turbine blade. Energy Conversion and Management. 2019;182:154-165.

16. Hara Y, Horita N, Yoshida S, Akimoto H and Sumi T. Numerical analysis of effects of arms with different cross-sections on straight-bladed Vertical Axis Wind Turbine. Energies. 2019;12:1-24.

17. Ismail MF and Vijayaraghavan K. The effects of aerofoil profile modification on a vertical axis wind turbine performance. Energy. 2015;80:20-31.

18. Lositaño ICM and Danao LAM. Steady wind performance of a 5 kW three-bladed H-rotor darrieus vertical axis wind turbine (VAWT) with cambered tubercle leading edge (TLE) blades. Energy. 2019;175:278-291.

19. Kim D and Gharib M. Efficiency improvement of straight-bladed vertical-axis wind turbines with an upstream deflector. Journal of Wind Engineering and Industrial Aerodynamics. 2013;115:48-52.

20. Kirke BK and Lazauskas L. Limitations of fixed pitch Darrieus hydrokinetic turbines and the challenge of variable pitch. Renewable Energy. 2011;36:893-897.

21. Zhang Y, Li Q, Zhu X, Song X, Cai C, Guo Z. Wind tunnel experiments and numerical study on performance characteristics of an H-type vertical axis wind turbine in the spanwise direction, Journal of Thermal Science. 2021;30(3):758-771.

22. Bangga G, Dessoky A, Wu Z, Rogowski K, Hansen MOL. Accuracy and consistency of CFD and engineering models for simulating vertical axis wind turbine loads. Energy. 2020;206:1-24.

23. Zhong J, Li J,Guo P, Wang Y. Dynamic stall control on a vertical axis wind turbine aerofoil using leading-edge rod. Energy, 2019;174:246-260.

24. Cai C, Zuo Z, Morimoto M, Maeda T, Kamada Y, LiuS. Two-step stall characteristic of an airfoil with a single leading-edge protuberance. AIAA Journal. 2018;56:64-77.